LAWRENCE
LIVERMORE
NATIONAL
LABORATORY

UCRL-PROC-207946

Pulse length dependence of laser conditioning and bulk damage in KD2PO4

J. J. Adams, T. L. Weiland, J. R. Stanley, W. D. Sell, R. L. Luthi, J. L. Vickers, C. W. Carr, M. D. Feit, A. M. Rubenchik, M. L. Spaeth, R. P. Hackel

November 11, 2004

Boulder Damage Symposium XXXVI, Annual Symposium on Optical Materials for High Power Lasers, 2004
Boulder, CO, United States
September 20, 2004 through September 22, 2004

UCRL-PROC-207946

Pulse length dependence of laser conditioning and bulk damage in KD_2PO_4

J. J. Adams*, T. L. Weiland, J. R. Stanley, W. D. Sell, R. L. Luthi, J. L. Vickers, C. W. Carr, M. D. Feit, A. M. Rubenchik, M. L. Spaeth, R. P. Hackel

Lawrence Livermore National Laboratory
7000 East Avenue, L-592
Livermore, CA 94550

ABSTRACT

An experimental technique has been developed to measure the damage density $\rho(\phi)$ variation with fluence from scatter maps of bulk damage sites in plates of KD_2PO_4 (DKDP) crystals combined with calibrated images of the damaging beam's spatial profile. Unconditioned bulk damage in tripler-cut DKDP crystals has been studied using 351 nm (3ω) light at pulse lengths of 0.055, 0.091, 0.30, 0.86, 2.6, and 10 ns. It is found that there is less scatter due to damage at fixed fluence for longer pulse lengths. The results also show that for all the pulse lengths the scatter due to damage is a strong function of the damaging fluence. It is determined that the pulse length scaling for bulk damage scatter in unconditioned DKDP material varies as $\tau^{0.24\pm0.05}$ over two orders of magnitude of pulse lengths. The effectiveness of 3ω laser conditioning at pulse lengths of 0.055, 0.096, 0.30, 0.86, 3.5, and 23 ns is analyzed in term of damage density $\rho(\phi)$ at 3ω, 2.6 ns. The 860 ps conditioning to a peak irradiance of 7 GW/cm^2 had the best performance under 3ω, 2.6 ns testing. It is shown that the optimal conditioning pulse length appears to lies in the range from 0.3 to 1 ns with a low sensitivity of 0.5 J/cm^2/ns to the exact pulse length.

Keywords: KDP, DKDP, laser conditioning, bulk damage, pulse length, pulse length scaling, damage density

1. INTRODUCTION

1.1 General

Currently, the only realistic choice for crystals for frequency conversion of large aperture kilo-joule class laser systems is KH_2PO_4 (KDP) and KD_2PO_4 (DKDP) [1]. Large boules (~250 Kg) can be grown that have good optical properties from which large aperture (~1600 cm^2) plates for frequency conversion can be fabricated [2]. Under frequency conversion conditions, crystals of KDP or DKDP can suffer from bulk and surface damage that would adversely affect the ability to focus the beam to a tight spot and endanger downstream optics. Realistically, unconditioned crystals of KDP and DKDP cannot be operated above approximately 5 J/cm^2, 351 nm (3ω), 3 ns peak without experiencing unacceptable bulk damage. This in turn limits the peak operational fluence of the laser system. However, treatment of the crystals with laser conditioning can improve the bulk damage performance of the crystals above the as-grown limit [3-5]. Laser conditioning is the increase in damage resistance that can occur through exposure to sub-damaging fluences. Specifically for this work, laser conditioning means "ramp" conditioning where the conditioning fluence is ramped in steps to just below the surface damage limit of the crystal or to the output limit of the laser used for the conditioning [5]. Figure 1 a.) is a scatter map image of a region of a DKDP crystal that had been exposed to a single shot at 8 J/cm^2 3ω, 3 ns and Figure 1 b.) is a scatter map image of a region that had first been ramped to 7 J/cm^2 in 1 J/cm^2 steps and then exposed to a single shot at 8 J/cm^2 3ω, 3 ns. The bright signals in the photos are scatter from bulk damage for side illumination with white light. The ramped region shows very little bulk damage as compared to the unconditioned region thus illustrating the effect of the "laser-conditioning". Historically, bulk damage and laser conditioning

* Correspondence: 925 422-4663, adams29@llnl.gov

effectiveness have both been observed to depend on pulse length [5,6]. This paper reports on a systematic and quantitative study of the pulse length dependence of bulk damage and laser conditioning.

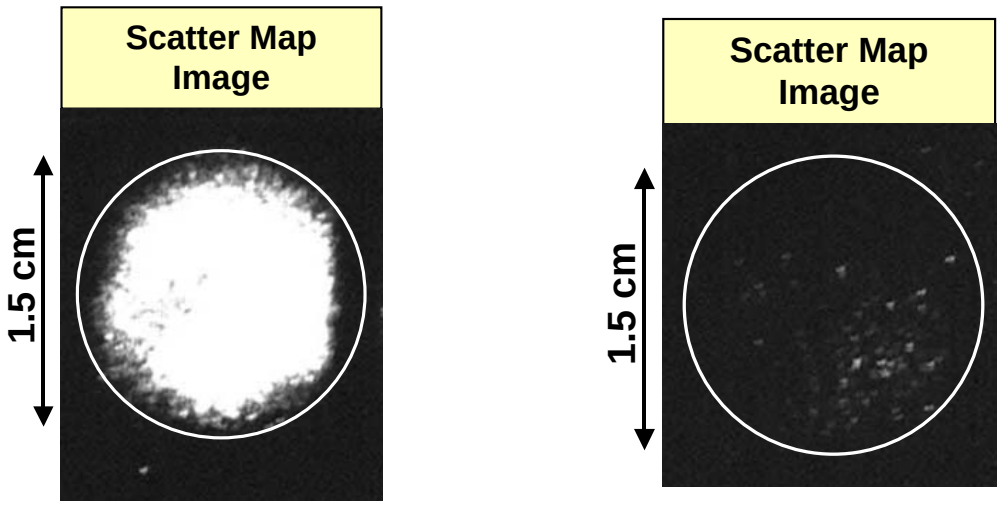

a.) b.)

Figure 1: Scatter map using side illumination with white light of a.) Unconditioned DKDP crystal exposed to a single shot at 8 J/cm^2 3ω, 3 ns. b.) Laser-conditioned DKDP crystal with a fluence "ramp" of 3, 4, 5, 6, 7 J/cm^2 3ω, 3 ns and then exposed to a single 8 J/cm^2 3ω, 3 ns test shot.

1.2 Study Goals

This study pursued three basic goals. First, a technique is developed to measure the damage density ($\rho(\phi)$) for bulk damage in unconditioned and laser-conditioned DKDP under testing at 3ω. Second, the pulse length dependence of bulk damage in unconditioned DKDP at 3ω is systematically studied and third, the effectiveness of 3ω laser conditioning at pulse lengths from 0.05-23 ns in DKDP is also systematically studied. This study of conditioning effectiveness at different pulse lengths reveals an optimum conditioning pulse length range. From the study of the pulse length dependence of unconditioned 3ω bulk damage, a pulse-scaling factor is derived for damaging pulse lengths in the range 0.05 – 10 ns.

2. EXPERIMENTS

2.1 Conditioning and Test Facilities

Many of the conditioning and bulk damage experiments were conducted in Lawrence Livermore National Laboratory's (LLNL) Optical Sciences Laser (OSL) facility [5]. OSL is a large aperture tripled-Nd:Glass laser that has an approximate output energy at 1053 nm (1ω) of 180 J. The 1ω beam is frequency-tripled using a Type II/Type II conversion scheme with KDP/DKDP crystals. The 3ω OSL beam has two nominal diameters depending on the choice of apertures in the 1ω section of the laser. The 3ω beam is image relayed to the sample from the tripling crystal and can have either a 1/e full-width of 3.3-cm or 1.2-cm at the sample depending on the choice of apertures. The beam spatial profile is nominally a "top-hat" (as seen in Figure 2a.) with a somewhat super-gaussian profile across its top 10%. This variation has proved invaluable in making the $\rho(\phi)$ measurements as will be discussed below. The beam typically has a 15% contrast. OSL also has the capability to operate at pulse widths from ~0.05 – 30 ns. Temporally, the pulse shape is nearly gaussian. Figure 2b.) shows a temporal measurement of a nominal 3 ns pulse. Typically, the OSL pulse durations have a ±10% variation from shot-to-shot. Also, unless otherwise stated, the fluences that will be reported for the OSL

shots will be the mean value for the fluence across the top-hat portion of the beam, which corresponds to approximately the top 10% of the beam.

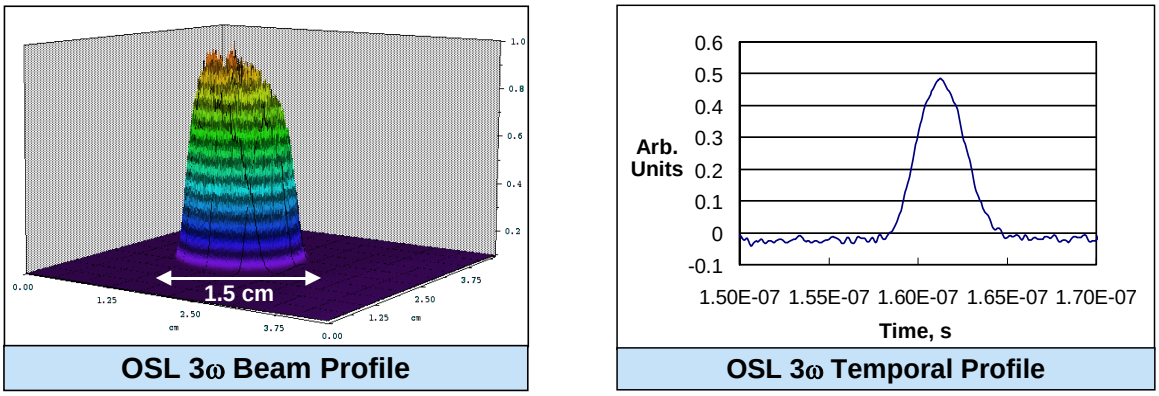

a.) b.)

Figure 2: a.) Spatial profile of the OSL beam at the sample plane for a 3ω 8 J/cm^2, 3 ns shot. b.) Photodiode trace of the temporal profile for a 3ω 8 J/cm^2, 3ns OSL shot.

The 3.5 ns and 23 ns laser raster-conditioning was accomplished in LLNL's Phoenix conditioning facility [5]. Figure 3 shows a schematic of the Phoenix facility, as it appeared when the work for this study was performed. The Phoenix laboratory utilizes two lasers to condition optics. A XeF excimer laser that operates at 351 nm with a pulse repetition frequency of 100 Hz is one of the available lasers. The excimer laser has an effective FWHM pulselength of ~23 ns and a maximum output energy of ~280 mJ [7]. The excimer beam is focused at the sample plane through the optics shown in Figure 3. An image of the excimer beam at the sample plane is shown in Figure 4 with the full-widths labeled. The depth of focus of the excimer beam at the sample is about 2 mm and the focus is typically positioned at the center of the part (in the direction of propagation). The excimer laser has excellent beam pointing stability and outputs a randomly polarized beam (50% horizontal and 50% vertical). A pair of polarizers was inserted into the excimer beam path to produce a horizontally polarized beam for use in the conditioning scans.

The other laser available in the Phoenix laboratory for conditioning is a tripled-Nd:YAG laser as shown in Figure 3. This laser is tripled to produce 355-nm light with a gaussian FWHM pulse length of 3.5 ns at 50 Hz and a maximum output energy at 355-nm of ~200 mJ. The YAG laser is brought to a far-field focus at the sample plane. An image of the focused YAG beam at the sample plane is shown in Figure 5. The horizontally polarized YAG laser beam at the sample plane has a 1/e^2 width of 420 μm. The depth of focus of the YAG beam at the sample is about 2 m. The YAG laser has poor pointing stability, in large part because it is used in the far-field.

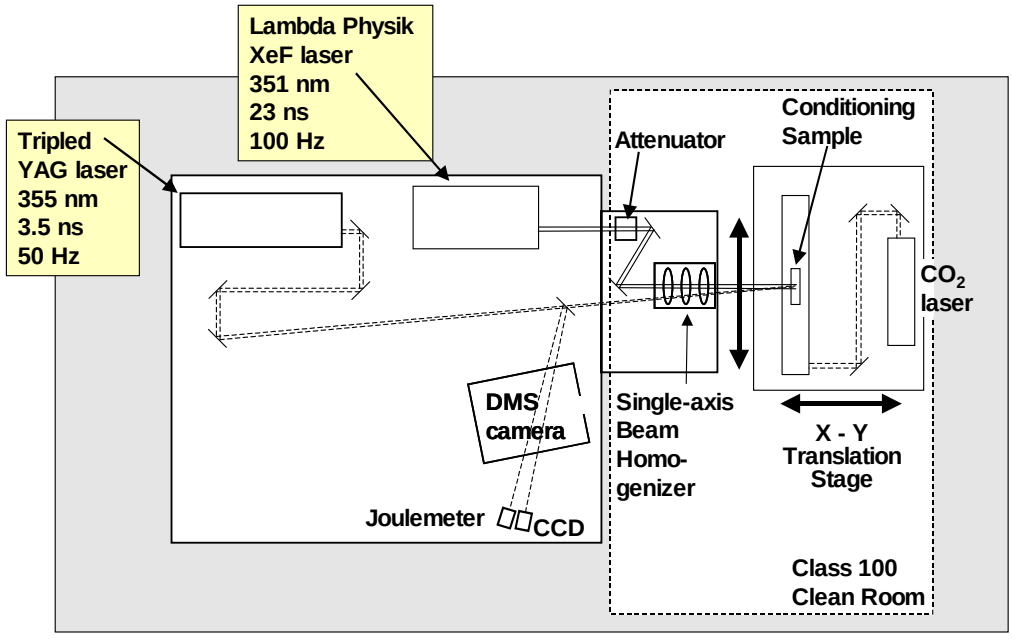

Figure 3: Experimental layout for the Phoenix conditioning facility [5].

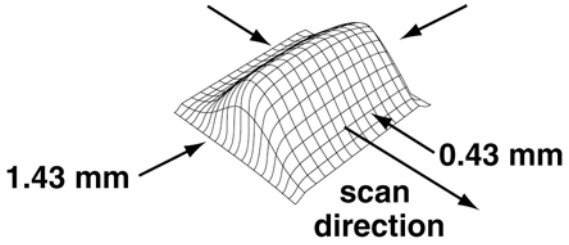

Figure 4: Spatial profile of the Excimer laser beam at the sample plane. The beam has an approximate flat-top profile in the long-axis (FW90%M of 1.43 mm) and a gaussian profile in the short-axis (FW1/e^2 of 0.43 mm).

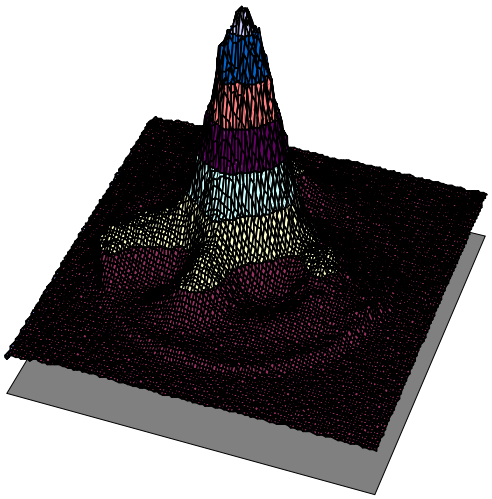

Figure 5: Spatial profile of the 355-nm, 3.5 ns YAG laser beam at the sample plane. The beam has an approximate gaussian spatial profile with a full-width at $1/e^2$ of 420 μm.

2.2 Experimental Plans

Two different types of experiments were performed. The samples used for the experiments were conventional growth DKDP oriented for type II tripling. 15 x 15 x 1-cm^3 plates were fabricated out of cut-offs of boule LL16 grown by Cleveland Crystals, Inc. for the National Ignition Facility (NIF). The surfaces of the samples were prepared with a diamond bit-turned finish. Two 15-cm samples were used in this study and will be denoted as LL16-1 and LL16-13.

The first set of experiments involved performing single-shot damage tests in OSL at 3ω using nominal pulse lengths of 40 ps, 100 ps, 300 ps, and 800 ps. The 1.5-cm OSL beam was used for these experiments where virgin regions of sample LL16-1 were exposed to single shots at progressively higher fluences (each on a different site on the crystal) at each pulse length. The sample was then scatter-mapped using a damage mapping system (DMS) [5,8] set-up which produced a digital image to be used to measure $\rho(\phi)$. The analysis to extract $\rho(\phi)$ will be discussed in the next section.

The second set of experiments was performed in two parts. First, virgin regions of crystal LL16-1 were ramp conditioned in OSL using the 3.5-cm beam at pulse lengths of 40 ps, 100 ps, 300 ps, and 800 ps and virgin regions of crystal LL16-13 were raster-scanned in Phoenix at pulse lengths of 3.5 ns or 23 ns. The nominal conditioning fluence ramps used in OSL at the pulse lengths of 40 ps, 100 ps, 300 ps, and 800 ps were 0.1, 0.2, 0.3 J/cm^2, 0.3, 0.6, 0.9 J/cm^2, 1.0, 2.0, 2.5, 3.0, 3.5, 4.0 J/cm^2, and 2, 3, 4, 5, 6 J/cm^2, respectively. The nominal conditioning fluence ramps used in Phoenix at the pulse lengths of 3.5 ns and 23 ns were 4, 5, 6, 7, 8, 9, 10 J/cm^2 and 14, 28 J/cm^2, respectively. A 90% fluence overlap was used in the raster-conditioning in Phoenix and 4 scans at each fluence was used. The second part of the experiment tested the conditioned regions of the crystals using the 1.5-cm beam in OSL. The testing consisted of single-shots at 3ω, 3ns with a fluence of ~ 12 J/cm^2. The samples were then scatter-mapped using a DMS set-up which produced a digital image to be used to measure $\rho(\phi)$. The analysis to measure $\rho(\phi)$ will be discussed in the next section.

2.3 Measuring $\rho(\phi)$

Bulk damage in crystals typically consists of small micro-cavities [6] which will be referred to as "pinpoints" and $\rho(\phi)$ denotes the density of these micro-cavities in terms of pinpoints per cubic millimeter. Figure 6 illustrates the process in which $\rho(\phi)$ measurements are extracted from actual damage sites on the crystals. Basically, an image of the damage (calibrated to $\rho(\phi)$ as will be discussed below) is combined with an image of the corresponding damaging beam's spatial profile (in units of fluence per pixel) to yield damage density (pinpoints/mm^3) vs. damaging fluence. The first step in the

process is to damage a site on a crystal and record an image of the damaging beam's spatial fluence profile. The next step (step 2 in Figure 6) is to obtain a calibrated scatter or damage map of the damaged site in the crystal. The damage map needs to be calibrated from counts per pixel to pinpoint density per pixel. The calibration of the damage map is accomplished by using an automated scanning microscope to count the pinpoints throughout the damage site in the crystal. The damaging beam's spatial profile is registered to the damage map collected from the crystal. The two images are scaled and rotated until features in the beam's spatial profile overlay with corresponding features in the damage map. The registered images are then divided into 5 pixel x 5 pixel subsets where the average fluence or pinpoint density is calculated in each subset throughout each image. We have determined that performing the average over 5 x 5 pixel subsets optimizes noise reduction without losing resolution. The third step is to plot corresponding registered pairs of average pinpoint density vs. average fluence to obtain the $\rho(\phi)$ curve. Figure 7 shows an expanded view of the $\rho(\phi)$ curve shown in Figure 6. This $\rho(\phi)$ is for unconditioned LL16 material damaged with a 7.5 J/cm^2 3ω, 3.4 ns pulse. The scatter in the $\rho(\phi)$ data is believed to be due to registration errors between the two images, focus error in the damage map, and possibly moderate scale non-uniformities in the crystal. It was determined that plotting the data as ordered (rather than x-y registered) pairs produces a smooth well-behaved curve though the center of the scatter in the x-y registered data. This curve is consistent with values found by fitting the unordered data. The ordering is carried out by first sorting the fluence data from lowest to highest value independent of the pinpoint data and then sorting the pinpoint data similarly. Then the two sets of data are put into one to one correspondence and plotted as shown in Figure 8. For the current work, this technique may be considered the equivalent of ensemble smoothing the data (which yields similar results). A study demonstrating the feasibility and utility of this technique will be the subject of a forthcoming publication. Note the data in Figure 7 and Figure 8 is the same data where Figure 7 is the registered pairs plot and Figure 8 is the ordered pairs plot. The ordered plot of the data as shown in Figure 8 is very close to a best fit to the data in Figure 7. The ordered pairs plot is a sensible way to present the $\rho(\phi)$ data if the damage density is an increasing function of the fluence, the majority of the error sources are random, and if the registration errors are not too large. The contribution to the scatter in the $\rho(\phi)$ plots derived in this study due to each of these has been investigated by the authors and it has been concluded that it is very reasonable to use the ordered data for analysis. Therefore the following analysis in this report will solely use the ordered pair data.

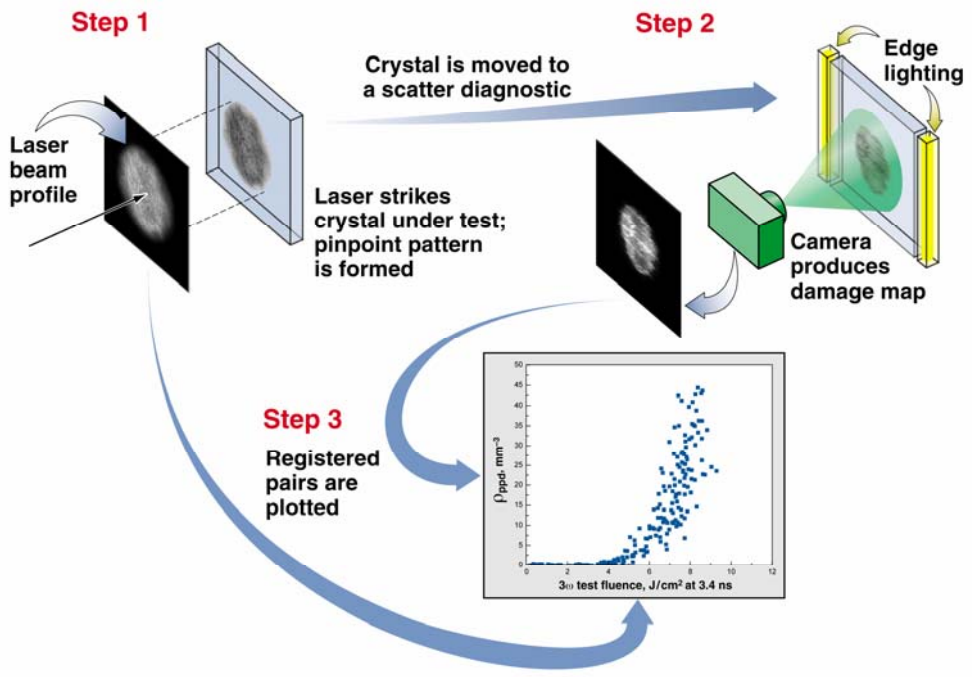

Figure 6: Process steps to extract $\rho(\phi)$ measurements from a scatter (damage) map image of the damage site and the corresponding damaging beam's spatial profile.

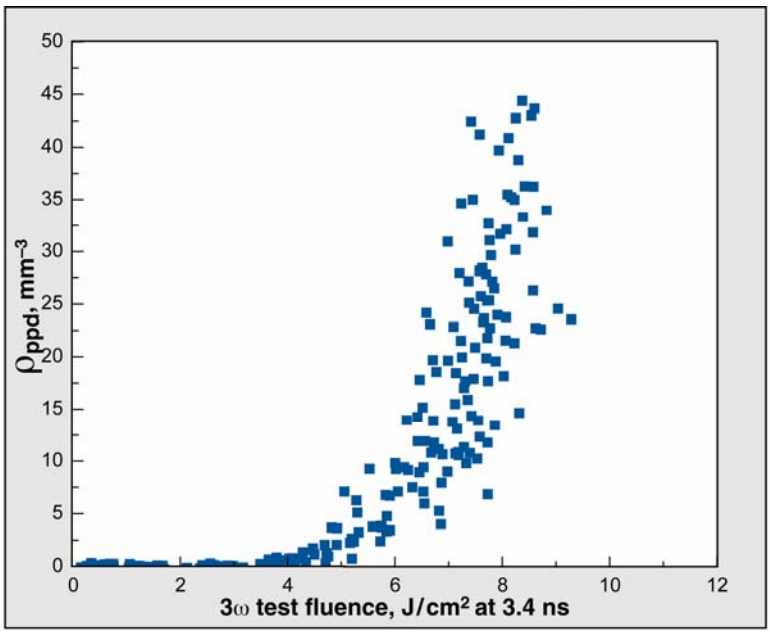

Figure 7: Plot of registered pairs of average fluence and pinpoint density extracted from the damaging beam and damage map images as described in Figure 6 for an unconditioned site on LL16-1 exposed to a 7.5 J/cm^2, 3ω, 3 ns shot.

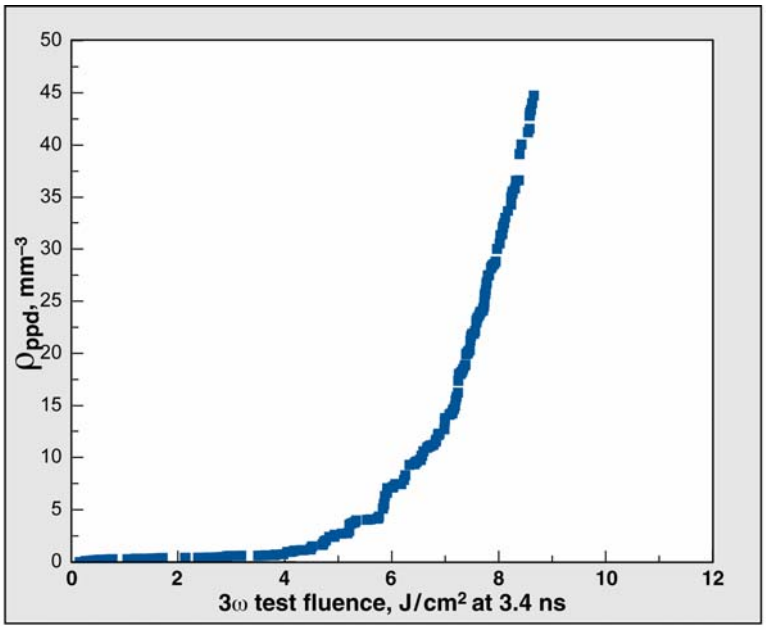

Figure 8: Plot of ordered pairs of average fluence and pinpoint density extracted from the damaging beam and damage map images as described in Figure 6 for an unconditioned site on LL16-1 exposed to a 7.5 J/cm^2, 3ω, 3 ns shot. The data shown here is the same data as in Figure 7 only that the pinpoint density and fluence values were independently sorted from lowest to highest value before plotting.

3. RESULTS AND ANALYSIS

3.1 Damage map of LL16-1

Figure 9 shows a damage map of crystal LL16-1 after single-shot damage testing at 3ω on both unconditioned and conditioned material. The single-shot damage testing was conducted with the 1.5-cm diameter beam. The ramp conditioning was performed using the 3.5-cm beam. The upper-half of the crystal was unconditioned and tested with single shots at pulse lengths from 0.04 – 10 ns. The lower half of the crystal had four regions that were conditioned at pulse lengths of ~0.8, 0.3, 0.1, and 0.04 ns. These regions are outlined with white boxes in Figure 9. An outline of the 3.5-cm beam can be seen in each region, which is due to laser cleaning of the surface of the crystal as the ramp conditioning was performed. The conditioned regions were then damaged tested at ~3ns as shown in the figure. A single site on the unconditioned region was also single-shot tested at 10 ns but is not shown in the figure. The fluences and pulse lengths are labeled in Figure 9 as described in the caption.

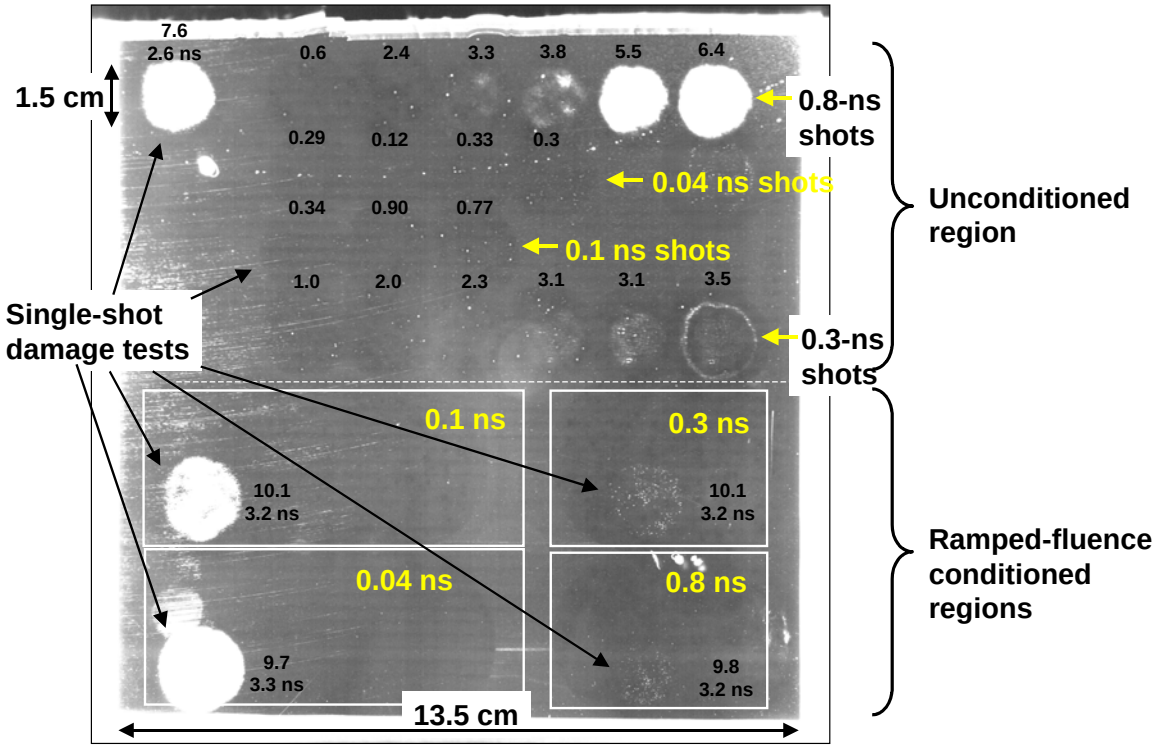

Figure 9: Damage map of DKDP crystal LL16-1 after conditioning and damage testing in OSL. The upper half of the crystal was unconditioned and exposed to single 1.5-cm diameter OSL shots with pulse lengths from 7.6 ns – 0.04 ns. The sub-nanosecond shots are arranged in rows of constant pulse length with the target pulse length for each row labeled on the right. For the four rows (0.8 – 0.04 ns shots), the numerical labels without units above each shot are the fluence for the shot. A single 1.5-cm diameter 2.6 ns test shot is labeled in the upper left corner. The lower half of the crystal was ramped-conditioned over four separate regions using the 3.5-cm OSL beam with pulse lengths of 0.04 – 0.8 ns. The white boxes outline the conditioned areas and the pulse length used for conditioning the area is labeled in each box. The conditioned areas were subsequently exposed to single 1.5-cm diameter ~3ns test shots where the fluence and pulse length is labeled to the right of each shot in the figure.

The faint horizontal lines running horizontally across the part are resulting from the vacuum chuck of the diamond-finishing machine. The arc of scattering sites running horizontally across the top quarter of the part is believed to been caused by chatter in the finishing tool. The large scattering site within the arc near the left-hand edge of the part is a fiducial applied to the part for use as a positioning aid during the OSL shots as are the three small scattering sites seen in a horizontal line near the top of the 0.8 ns conditioned region. The small circular scatter feature at 11 o'clock to the 9.7 J/cm^2, 3.3 ns test shot on the 40 ps conditioned region is a glove smudge. The "ring-like" appearance of the 3.5 J/cm^2, 0.3 ns test shot is due to the 1ω drive in OSL exceeding the optimum 3ω conversion point of the system thereby causing the edges of the beam to have higher conversion than its center. Upon inspection by "eye", it can be seen that the 0.8 and 0.3 ns conditioned regions performed substantially better under testing at ~10 J/cm^2, 3 ns than did either the 0.1 ns or 0.4 ns conditioned regions. Crystal LL16-13 was prepared, tested, and analyzed in a similar manner at 23 ns and 3 ns.

3.2 Unconditioned results

3.2.1 ρ(ϕ) (scatter vs. fluence)

Analysis of the test shots on the unconditioned region of LL16-1 to determine ρ(ϕ) at each pulse length was performed as described in section 2.3. However, due to the small (<1 μm) size of the pinpoints for pulse lengths at and below 300 ps, attempts to accurately count the pinpoints with the automated microscope failed and so the calibration of the scatter maps to pinpoint density for these pulse lengths could not be accomplished. It was still possible to perform the image analysis described in section 2.3, with the exception that instead of a plot of pinpoint density vs. fluence the resulting plot is scatter vs. fluence. Scatter is a very useful quantity in itself since it describes the amount of light lost out of the beam due to, in this case, bulk damage. It was decided to present data for the unconditioned damage testing at all pulse lengths in terms of scatter vs. fluence for consistency. Figure 10 shows the results for scatter vs. test fluence for the single-shot damage testing of unconditioned material on LL16-1 at 6 different pulse lengths. Figure 10 reveals that there is less scatter at a fixed fluence for longer pulse lengths. The results also show that at all of the pulse lengths the damage or scatter is a strong function of the damaging fluence.

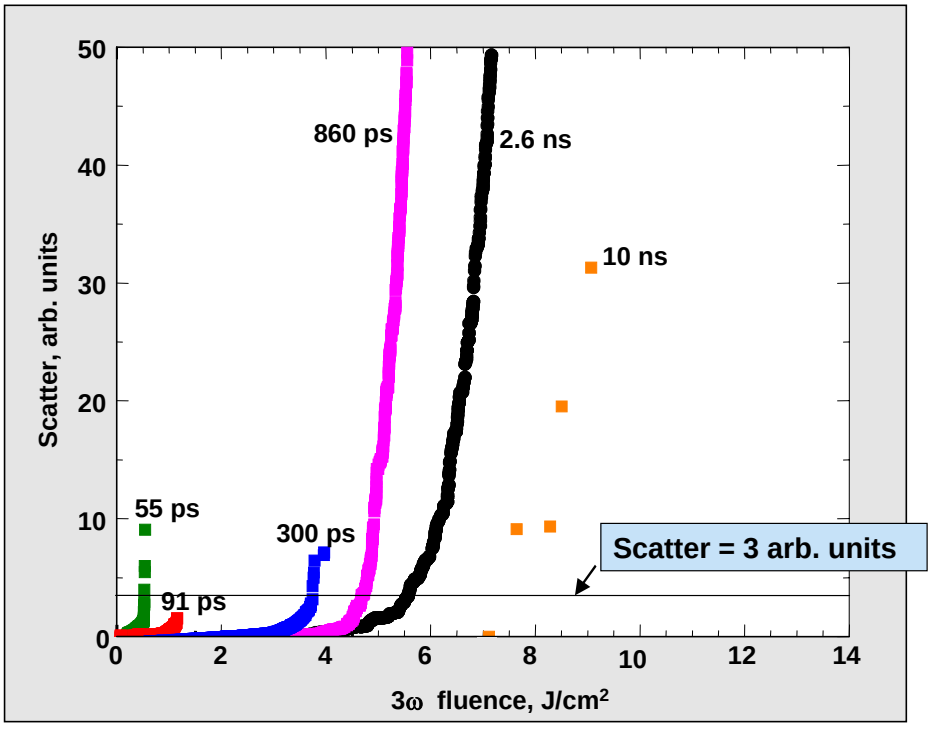

Figure 10: Plot of ordered pairs of average scatter vs. fluence extracted from the damaging beam and damage map images as described in section 2.3 for single-shot damage tests at six pulse lengths on the unconditioned region of LL16-1. Analysis of the 7.6 J/cm^2 2.6 ns, 5.5 J/cm^2 860 ps, 3.1 J/cm^2 300 ps, 0.90 J/cm^2 91 ps, 0.33 J/cm^2 55 ps, and the 12.5 J/cm^2 10 ns (not shown in Figure 9) shots is presented. The scatter equal to 3 arbitrary units is denoted to reference the scatter level used for the pulse scaling derivation.

3.2.2 Pulse scaling

The results shown in Figure 10 allow derivation of a fluence pulse length-scaling factor for equivalent pinpoint scatter over 2 orders of magnitude of test pulse lengths. The fluence corresponding to the scatter equal to 3 arb. units at each pulse length in Figure 10 is a convenient point to use to derive the pulse scaling relationship. Figure 11 shows a plot of the fluences corresponding to the scatter equal to 3 arbitrary units from Figure 10. The line through the data is a numerical fit of $a\tau^b$ where a and b are fitting parameters. The result of the fit is a pulse-scaling relationship of $\tau^{0.24 \pm 0.05}$ with the error to the exponent was found with curve fitting software. This is the first systematic determination of fluence pulse length scaling for equivalent pinpoint scatter over a wide range of test pulse lengths. A pulse scaling relationship of $\tau^{0.24}$ is plausible if the initiating absorbers have a distribution of finite sizes and their absorptivity varies with their size [9]. This pulse scaling result is also very consistent with results from by Runkel et al. that studied pulse scaling over a narrower range of pulse lengths [6]. Other levels of scatter were used for pulse lengths where data was available in the same manner to derive the pulse scaling relationship and the results for the exponent agreed with that shown in Figure 11 to within ±0.01.

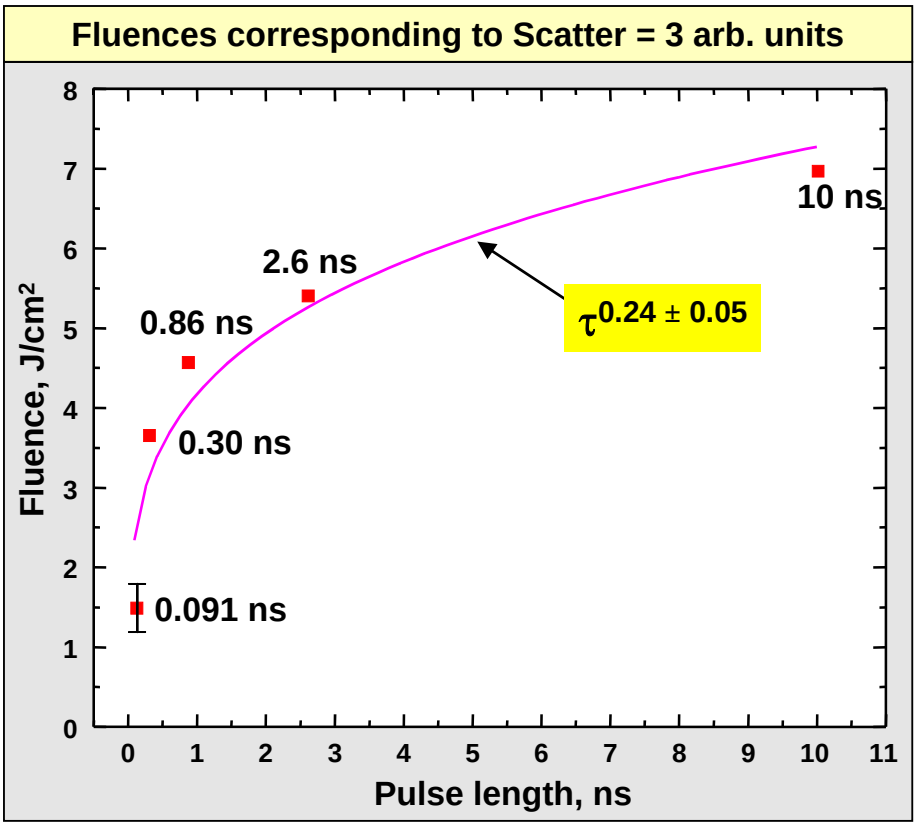

Figure 11: Plot of fluence corresponding to scatter equal to 3 arbitrary units from Figure 10 for the test pulse lengths as labeled. The line is a numerical fit of $a\tau^b$ to the data. The result of the fit is a pulse-scaling relationship of $\tau^{0.24 \pm 0.05}$.

3.3 Conditioned results

3.3.1 ρ(ϕ)

Analysis of the 3ω, ~3 ns test shots on the conditioned regions of LL16-1 and LL16-13 to determine ρ(ϕ) was performed as described in section 2.3. Figure 12 shows the results for ρ(ϕ) vs. 3ω, 2.6 ns test fluence for the single-shot damage testing of the 0.8, 0.3, 0.1, and 0.04 ns conditioned regions on LL16-1 and for the 23 ns and 3.5 ns raster-scanned regions (as described in section 2.2) on LL16-13. Also shown in Figure 12 for comparison are the results from the testing of the unconditioned material on LL16-1 at 3ω, 2.6 ns. The results show that at all of the pulse lengths the damage density is again a strong function of the damaging fluence. The labels for the various curves specify the *conditioning* pulse length for the region tested as well as the measured peak irradiance obtained during the conditioning ramp. For the 23 ns and 3.5 ns cases, surface damage limited the peak irradiance to the values shown. For the conditioning pulse lengths of 55 ps – 860 ps, the plan was to ramp to 10 GW/cm^2 at each pulse length but instabilities and limits to the 3ω output of OSL produced the variety in peak intensities shown. However, the differences in peak conditioning intensities obtained do not severely affect the overall conclusions that can be drawn from these results. As can be seen in Figure 12, the 860 ps, 7 GW/cm^2 conditioned material had the best performance. Under 55 ps conditioning, the performance was essentially the same as unconditioned but as the conditioning pulse length increased to 860 ps the performance of the conditioned material progressively increased to an apparent maximum. Then as the conditioning pulse length further increased to 23 ns, the performance of the conditioned material decreased towards that of the unconditioned material. This behavior implies that there is a local maximum at approximately 860 ps in the performance of conditioned material for these conditioning parameters.

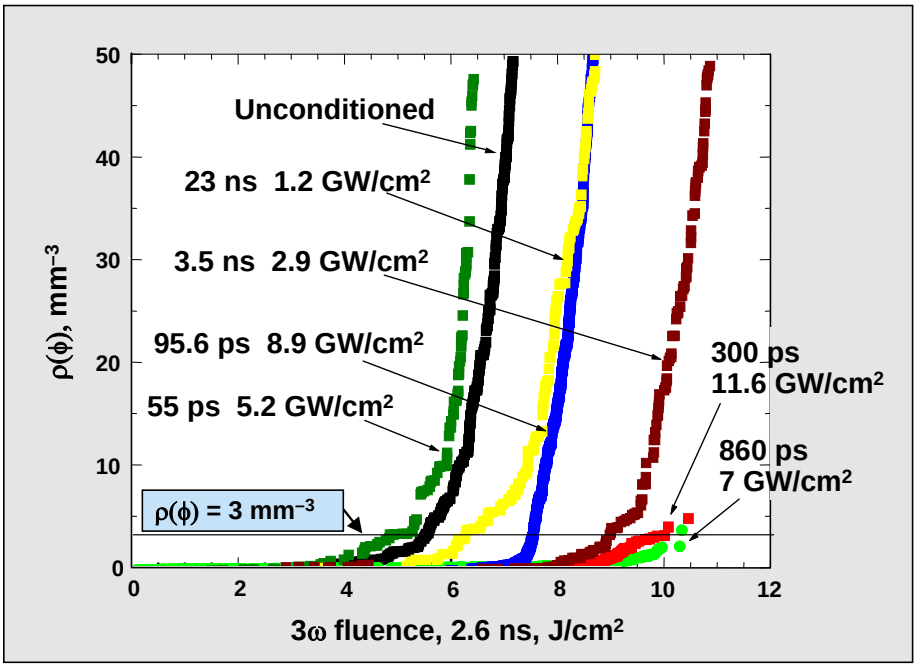

Figure 12: Plot of ordered pairs of average scatter vs. fluence extracted from the damaging beam and damage map images as described in section 2.3 for single-shot damage tests at 3ω, 2.6 ns on the conditioned regions of LL16-1 (Figure 9) and LL16-13. The labels give the pulse length used for the *conditioning* and the peak irradiance achieved during the conditioning ramp. The unconditioned data is shown for comparison. The calibration to pinpoints/mm^3 for the 55, 95.6, and 860 ps data was estimated from the available calibration data at the other pulse lengths. The scatter equal to 3 arbitrary units is referenced for the discussion of differences in the performance of the various pulse length conditioned material.

3.3.2 Optimal conditioning pulse length

To better reveal the apparent maximum in damage performance of the conditioned material near 860 ps, Figure 13 shows a plot of test fluences corresponding to $\rho(\phi) = 3$ ppts/mm^3 vs. conditioning pulse length from Figure 12. The level for unconditioned damage performance is as labeled. Figure 13 shows that there appears to be an optimal range for the conditioning pulse length between about 0.3 – 1 ns and in this range the sensitivity of the shift in fluence of the $\rho(\phi)$ curves after conditioning to variation in pulse length is low (0.5 J/cm^2/ns). The local maximum on Figure 13 implies that the level of conditioning obtained at a given pulse length is a function of both the fluence and irradiance applied to the material. The fall-off in performance of the conditioned material for conditioning pulse lengths <800 ps is believed by the authors to be due to the reduction in the fluence applied to the material at the shorter conditioning pulse lengths. Note that in the 860 ps, 7 GW/cm^2 case, 6 J/cm^2 was applied to the material, in the 300 ps, 11.6 GW/cm^2 case, 3.5 J/cm^2 was applied to the material, and in the 95.6 ps, 8.9 GW/cm^2 case, 0.85 J/cm^2 was applied to the material all at equal beam diameters. Since these intensities are roughly equivalent, this implies that the reduction in *fluence* applied at the shorter pulse lengths is the cause of the reduced conditioning effect. The optimal conditioning pulse length range identified here therefore corresponds to the range of ideal combinations of fluence and intensity to obtain maximum conditioning for 3ω, 2.6 ns induced damage. For conditioning pulse lengths >3 ns, surface damage limits the maximum conditioning irradiance which implies that the fall-off in the performance of the >3ns conditioned material seen here is reasonable and important from a practical point of view.

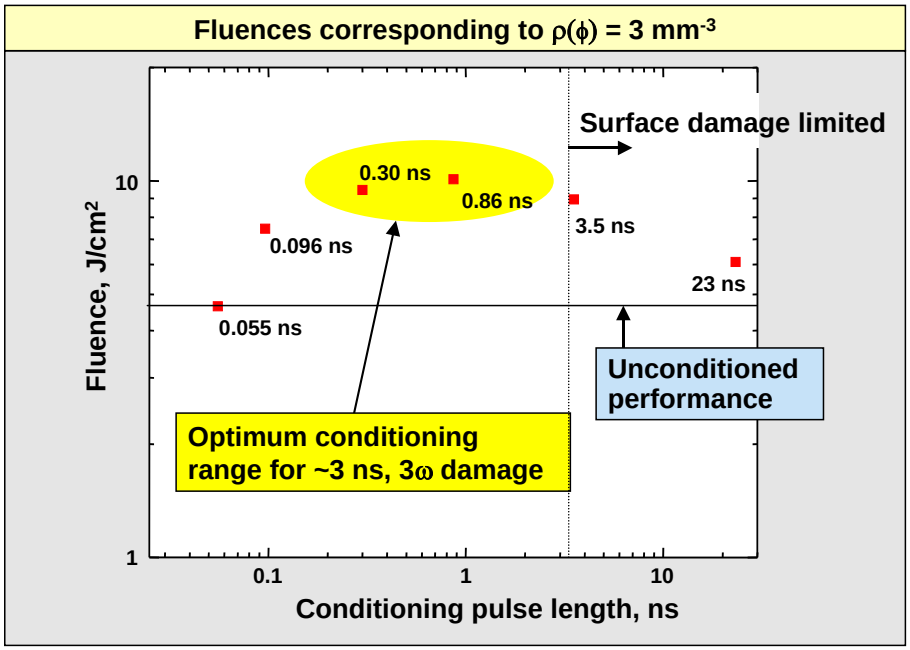

Figure 13: Plot of 3ω, 2.6 ns test fluences corresponding to $\rho(\phi) = 3$ ppts/mm^3 for the various conditioning pulse lengths from Figure 12. The exact conditioning pulse lengths are labeled on the figure. The optimal pulse length range for conditioning for 3ω, 2.6 ns damage appears to be 0.3 – 1 ns.

4. SUMMARY

A method to quantify bulk damage in plates of DKDP crystals in terms of scatter and damage density $\rho(\phi)$ has been developed. Performance of unconditioned material was studied in terms of scatter vs. damaging fluence at 3ω damaging pulse lengths of 0.055, 0.091, 0.30, 0.86, 2.6, and 10 ns. It was found that there is less scatter at fixed fluence for longer pulse lengths. The results also show that at all pulse lengths the damage density or scatter is a strong function of the damaging fluence. From the unconditioned data, it is further determined that damage fluence for equivalent scatter scales as $\tau^{0.24 \pm 0.05}$ over two orders of magnitude of pulse lengths and is consistent with past work by other authors [6]. Damage densities $\rho(\phi)$ for material tested at 3ω, 2.6 ns after conditioning at 0.055, 0.096, 0.30, 0.86, 3.5 and 23 ns were measured and used to quantify the degree of conditioning. The results show that the damage density for conditioned material is again a strong function of the damaging fluence. The material conditioned at 860 ps to a peak irradiance of 7 GW/cm^2 had the best performance under 3ω, 2.6 ns testing. A relatively broad maximum in the performance of the various pulse length conditioned material was observed between 0.3 and 1 ns with a low sensitivity (derivative) to the conditioning pulse length of 0.5 J/cm^2/ns. The optimal conditioning pulse length range for 3ω, 2.6 ns induced damage therefore appears to be 0.3 – 1 ns. It was determined that at equal conditioning irradiance, the decrease in the conditioning effectiveness for conditioning pulse lengths <800 ps was a result of lower fluence applied to the material at the shorter conditioning pulse lengths. Surface damage was found to limit the peak conditioning irradiance for conditioning pulse lengths >3 ns.

ACKNOWLEDGEMENTS

The authors wish to thank Mike Nostrand for his assistance with the $\rho(\phi)$ measurements, and Eric Miller and Heather Platz for cleaning and coating the crystals used in this work, all with LLNL. This work was performed under the auspices of the U.S. Department of Energy by the University of California, Lawrence Livermore National Laboratory under contract No. W-7405-Eng-48.

REFERENCES

1. J. J. De Yoreo, A. K. Burnham, P. K. Whitman, "Developing KH_2PO_4 and KD_2PO_4 crystals for the world's most powerful laser," Int. Mater. Rev. **47**, 113 (2002)
2. N. P. Zaitseva, J. Atherton, R. Rozca, L. Carmen, I. Smolsky, M. Runkel, R. Lyon, and L. James, J. of Crystal Growth **197**, 911 (1999)
3. M. Runkel, S. Maricle, R. Torres, J. Auerbach, R. Floyd, R. Hawley-Fedder, and A. Burnham, "Effect of thermal annealing and second harmonic generation on bulk damage performance of rapid growth KDP type I doublers at 1064 nm", 2000 SPIE Proceedings, **4347**, 389 (2001)
4. M. Runkel, K. Neeb, M. Staggs, J. Auerbach, A. K. Burnham, "The results of raster-scan laser conditioning studies on DKDP triplers using Nd:YAG and excimer lasers," 2001 SPIE Proceedings, **4679**, 368 (2002)
5. M. Runkel, J. Bruere, W. Sell, T. Weiland, D. Milam, D. Hahn, M. Nostrand, "Effects of pulse duration on bulk laser damage in 350-nm raster scanned DKDP," 2002 SPIE Proceedings, **4932**, 405 (2003)
6. M. Runkel, A. K. Burnham, D. Milam, W. Sell, M. Feit, A. Rubenchik, "The results of pulse-scaling experiments on rapid-growth DKDP triplers using the Optical Sciences Laser at 351 nm," 2000 SPIE Proceedings, **4347**, 359 (2001)
7. M. Runkel, "Some commonly used calculations in small beam damage testing: Effective area, effective pulse durations, and pulse scaling," NIF report # (October 1, 2002)
8. F. Rainer, "Mapping and inspection of damage and artifacts in large-scale optics," 1996 SPIE Proceedings, **3244**, 272 (1997)
9. M. D. Feit and A. M. Rubenchik, "Implications of nanoabsorber initiators for damage probability curves, pulse length scaling, and laser conditioning," 2003 SPIE Proceedings, **5273**, 74 (2004)